RSC Advances

ROYAL SOCIETY OF CHEMISTRY

www.rsc.org/advances

Journal Name

COMMUNICATION

Rapid and high-yield production of g-C_3N_4 nanosheets via chemical exfoliation for photocatalytic H_2 evolution †

Received 00th January 20xx,
Accepted 00th January 20xx

DOI: 10.1039/x0xx00000x

www.rsc.org/

Jincheng Tong, Li Zhang,* Fei Li, Ke Wang, Lifen Han and Shaokui Cao*

Rapid and high-yield production of graphitic carbon nitride (g-C_3N_4) nanosheets was realized by simply adding water into H_2SO_4 suspension of bulk g-C_3N_4, and as-prepared nanosheets exhibit enhanced photocatalytic H_2 evolution. Notably, the degree of exfoliation can be controlled by the amount of water to facilitate diverse application of nano-sized g-C_3N_4.

Graphitic carbon nitride (g-C_3N_4), a metal-free polymer semiconductor with a typical layered structure, has been studied as a prospective material in varied areas such as heterogeneous catalysis,[1-3] fuel cells,[4, 5] photocatalytic water splitting[6, 7] and photodegradation of pollutants,[8] owing to its abundance, stability and chemical tunability[9]. Analogue to 2D atom-thick graphene, which presents many intriguing properties different from bulk graphite and potential in diverse application, the ultrathin g-C_3N_4 nanosheets can be obtained by the delamination of their bulk layered counterparts, and these resulting g-C_3N_4 nanosheets exhibit exotic electronic property and high surface area accompanied by greatly enhanced host capabilities due to its high 2D anisotropy and quantum confinement effects, which have triggered a wide range of new applications including anomalous piezoelectricity,[10] bioimaging,[11] sensing[12, 13] and memory device[14]. In view of the significance of g-C_3N_4 nanosheets, great efforts have recently been devoted to preparing g-C_3N_4 ultrathin nanosheets and exploring their novel properties. For instance, g-C_3N_4 nanosheets can be synthesized by opening the stacked layers of bulk through either thermal oxidation etching or liquid exfoliation in polar solvents.[11, 13, 15, 16] However, these methods always give an extremely low yield and the liquid exfoliation strategy also needs a long time of sonication treatment (>10 h). Although the ultrasonic exfoliation time can be shortened by the use of strong acid through prior intercalation or protonation,[12, 17] the overall fabrication processes still suffer from complexity and low exfoliation efficiency. We have lately proposed a moderate exfoliation approach using diluted H_2SO_4 as an "efficient knife" to produce large-aspect-ratio g-C_3N_4 nanosheets with high final yield (60%). But the involved acid treatment and ultrasonic process are still cumbersome and the obtained nanosheets show limited dispersion stability and tend to reunite after a few days.[18] On the other hand, several pioneering works revealed that bulk g-C_3N_4 could be high-efficiently exfoliated and dissolved in acidic solvents under strong oxidizing acids and heat treatment,[19-21] nevertheless the extent of chemical exfoliation was difficult to control and hence it is prone to cause excessive disintegration and destroy the crystalline structure of g-C_3N_4. Therefore, more facile and effective methods for preparing well-dispersed ultrathin g-C_3N_4 nanosheets with high quality and large quantity are highly desirable.

Herein, we demonstrate our recent finding that g-C_3N_4 could be rapidly disintegrated and exfoliated in concentrated H_2SO_4 when water was dropwise added. Thus, for the first time, we obtained g-C_3N_4 nanosheets in a very short time (less than 30min). Remarkably, the final yield of the nanosheets after removing unexfoliated residual was up to 70%. This facile exfoliation method is readily scalable and leads to g-C_3N_4 nanosheets with uniformly distributed size (80 nm), which show significantly enhanced photocatalytic activity for visible light driven H_2 evolution from water.

The g-C_3N_4 nanosheets were prepared by directly adding certain amount of water dropwise into the mixture of bulk g-C_3N_4 and concentrated H_2SO_4 under ambient conditions. By controlling the water dropping speed to maintain the temperature at 60 °C, the yellow bulk g-C_3N_4 was quickly disintegrated and exfoliated into white g-C_3N_4 nanosheets with the final yield of 70% (see ESI for details). As illustrated in Fig. 1a, the obtained g-C_3N_4 nanosheets could be easily redispersed in water and the aqueous dispersion was highly stable without aggregation upon standing for more than 2 months. Furthermore, the well-defined Tyndall effect in the dispersion revealed the presence of highly monodisperse ultrathin g-C_3N_4 nanosheets in water.[11] The morphology of as-prepared g-C_3N_4 nanosheets was observed via AFM, SEM and TEM. In the AFM image (Fig. 1b), the randomly measured nanosheets have almost the same thickness (2.5 nm), indicating the bulk g-C_3N_4 was successfully exfoliated into ultrathin nanosheets. The presence of a few nanosheets with a thickness of 5.0 nm presumably corresponds

School of Materials Science and Engineering, Zhengzhou University, Zhengzhou 450052, China. E-mail: lizhang9@zzu.edu.cn, caoshaokui@zzu.edu.cn.

† Electronic Supplementary Information (ESI) available: Details of experimental section, additional characterizations (XPS spectra, Zeta potential, Photos, PL, FTIR and DRS spectra). See DOI: 10.1039/x0xx00000x

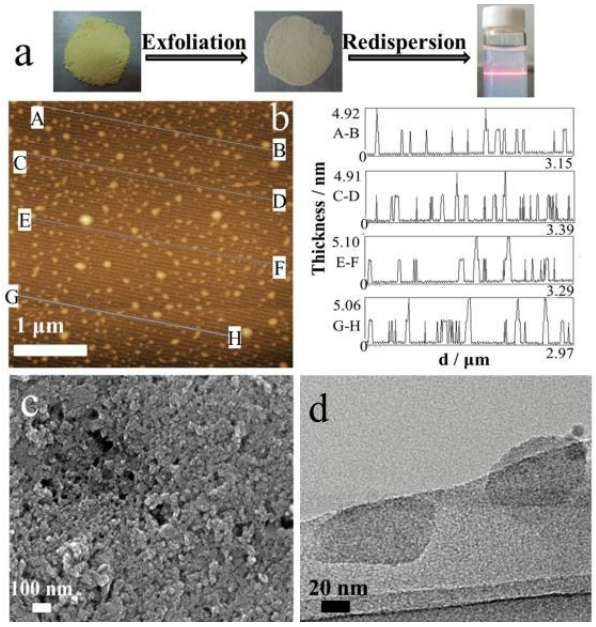

Fig. 1 (a) Photos of bulk g-C_3N_4, g-C_3N_4 nanosheets and the aqueous dispersion of the nanosheets. (b) AFM image of g-C_3N_4 nanosheets and the corresponding height profiles of four randomly chosen sections. (c) SEM image and (d) TEM image of g-C_3N_4 nanosheets.

to the overlapping of the nanosheets or folds and wrinkles on the nanosheets.[22, 23] The size distribution of as-prepared g-C_3N_4 nanosheets was evaluated by measuring the diameter of 100 nanosheets from the AFM image. As displayed in Fig. S1†, the diameter of the nanosheets ranges from 30 to 190 nm and the average diameter is 80 nm. The SEM image (Fig. 1c) further confirms that the lateral size of the g-C_3N_4 nanosheets is about 100 nm, which is much smaller than that of bulk g-C_3N_4 (Fig. S2a†). The representative TEM image in Fig. 1d illustrates the almost transparent feature of the two individual nanosheets with a diameter of ~80 nm, indicating the ultrathin thickness of the nanosheets compared with the opaque bulk counterpart (Fig. S2b†). As a result of the fully exfoliation, g-C_3N_4 nanosheets have larger specific surface area (86.29 $m^2 g^{-1}$) than bulk g-C_3N_4 (13.82 $m^2 g^{-1}$).

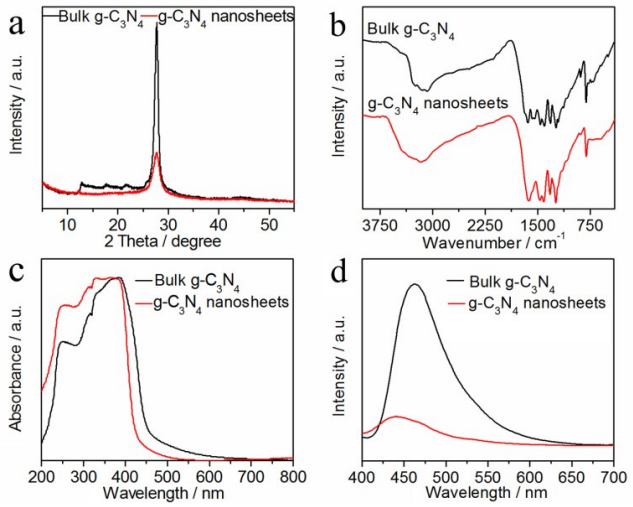

Fig. 2 (a) XRD patterns, (b) FTIR spectra, (c) UV-Vis DRS spectra and (d) PL spectra of bulk g-C_3N_4 and g-C_3N_4 nanosheets.

From the XRD patterns (Fig. 2a), typical diffraction peaks of bulk g-C_3N_4 can be observed in g-C_3N_4 nanosheets, implying the basic g-C_3N_4 atomic structure are largely retained. The strong XRD peak at 27.7°, originated from the (002) interlayer diffraction of graphite-like structures, sharply decrease for g-C_3N_4 nanosheets in comparison with that of bulk g-C_3N_4, suggesting the few-layered morphology after successful exfoliation.[16] Coupled with the AFM analysis (2.5 nm in thickness), the g-C_3N_4 nanosheets are calculated to be composed of 7 atomic monolayers.[11] The low-angle diffraction peak at 12.8°, derived from in-planar repeated tri-s-triazine units, also become less pronounced for the nanosheets, mainly due to simultaneously decreased planar size of the g-C_3N_4 layers during the exfoliation process.[16, 17] The characteristic FTIR spectrum of the g-C_3N_4 nanosheets is similar to that of the bulk material (Fig. 2b), both having peaks at 810 cm^{-1} (tri-s-triazine ring), 900-1800 cm^{-1} (aromatic CN heterocycles containing either trigonal $N(-C)_3$ or bridging C-NH-C units) and 3000-3500 cm^{-1} (uncondensed terminal amino groups). Nevertheless, the intensity and position of vibration peaks in the range of 900-1800 cm^{-1} for the nanosheets are slightly changed with respect to those of bulk g-C_3N_4, which may result from the protonation and disintegration of g-C_3N_4.[21, 24] The structural resemblance between nanosheets and bulk g-C_3N_4 is further confirmed by XPS (Fig S3a†). The weak O singals in the XPS survey spectra can be ascribed to the absorbed oxygen species on sample surface, and the slightly higher O peak for nanosheets may be due to their high specific surface area and protonation by H_2SO_4.[11, 21] The C 1s spectra (Fig. S3b†) show one predominant C1 peak at 288.0 eV for both nanosheets and bulk g-C_3N_4, corresponding to the sp^2-bonded carbon in g-C_3N_4 network. The C2 peak at 284.6 eV is related to carbon contamination.[17] Meanwhile, four deconvoluted N 1s peaks (N1-N4) assigning to C=N-C, $N(-C)_3$, C-N-H and charging effect respectively, are observed for both nanosheets and bulk g-C_3N_4 (Fig S3c†). The slightly increased intensity of N4 and N3 for the nanosheets may result from the protonation of nanosheets with H_2SO_4 and dissociation of bridging bond -NH- between tri-s-triazine units.[12, 24, 25] Besides, a new S 2p component located at 168.4 eV is observed for g-C_3N_4 nanosheets, which falls within the range of energies characteristic of SO_4^{2-} (Fig S3d†), also proving protonation of the nanosheets.[21] The protonation process is further evidenced by zeta-potential measurement of the g-C_3N_4 nanosheets dispersion in water, which is shifted to +4.96 mV compared with -22.2 mV of bulk g-C_3N_4 (Fig S4†).

It was observed from the UV-Vis diffuse reflectance spectra (DRS) that the intrinsic absorption edge of g-C_3N_4 nanosheets exhibits blue-shift from 453 nm to 423 nm with the bandgap increasing from 2.74 eV of bulk g-C_3N_4 to 2.93 eV of nanosheets (Fig. 2c). Correspondingly, the emission peak of the nanosheets shifts from 464 to 433 nm relative to bulk g-C_3N_4 as illustrated in their photoluminescence (PL) spectra (Fig. 2d). The larger bandgap and blue-shift of fluorescence can be attributed to the quantum confinement effect with the conduction and valence band shifting in opposite directions.[15]

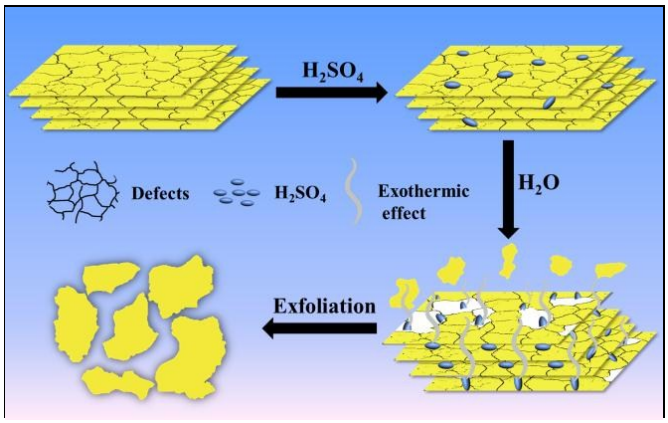

Fig. 3 Schematic illustration of the exfoliation process of g-C_3N_4.

To elucidate the formation mechanism of g-C_3N_4 nanosheets, we monitored the exfoliation process of bulk g-C_3N_4 with adding different amount of water into the suspension consisted of bulk g-C_3N_4 and concentrated H_2SO_4. As seen in Fig. S5†, adding the first 5 mL water turned the colour of suspension from yellow to white and consequently g-C_3N_4 nanosheets were obtained at this stage. When further add the second 5 mL water, the suspension became almost transparent, but still showed the obvious Tyndall effect, suggesting that smaller-sized g-C_3N_4 fragments were formed in the second stage. Generally, the luminescence property of the carbon nitride materials is considered mainly effected by the size of the sp^2 C-N clusters and the lone-pair (LP) electrons of the nitride.[25, 26] This transparent suspension was found to have two PL emission peaks at 410 nm and 464 nm (Fig. S6†), which could be attributed to the σ*→LP transition and π*→LP transition respectively, indicating the appearance of energy-band splitting probably caused by disintegrating g-C_3N_4 framework into smaller-sized sp^2 C-N clusters during further water adding process.[26-28] Moreover, these smaller-sized g-C_3N_4 fragments could be further separated according to the degree of exfoliation by successively precipitating the transparent suspension (Fig. S5c†) using different poor solvents such as water and ethanol. As described in section S3 in ESI, the precipitate obtained from water (P1) has a lower degree of exfoliation compared to the successive precipitate from ethanol (P2). The FTIR spectra were conducted to reveal how the chemical structure varies throughout the whole exfoliation process (Fig. S7†). Compared to bulk g-C_3N_4, there are some band changes in the spectra of nanosheets and precipitates: the blue-shift of N-H signals (3000-3500 cm^{-1}) and emergence of new signals assigned to -NH_2 group (3336, 613 and 457 cm^{-1}) suggest the dissociation of hydrogen-bonds between polymeric tris-s-triazine units with NH/NH_2 groups,[29, 30] the decrease of signal intensities in low-wavenumber fingerprint region related to bridging C-NH-C units (1205, 1236 and 1313 cm^{-1}) and the concomitant increase of signal intensities linked to oxygen-containing groups (1712, 1088 and 972 cm^{-1}) indicate the cleavage of bridging bond -NH- between tri-s-triazine units due to the hydrolysis/oxidation during in the exfoliation process.[24, 27, 31] It has been known that the polymeric g-C_3N_4 generally possesses some structural defects such as primary or secondary amino groups due to incomplete condensation of tris-s-triazine units,[24, 25] and as-obtained g-C_3N_4 might be broken up from these defects by protonation or oxidation[20, 32, 33] (Fig. S8†). Furthermore, these FTIR band changes become more evident with adding more water, revealing that g-C_3N_4 is exfoliated stepwise during adding water process. This is also supported by DRS results (Fig. S9†), which show the sequentially blue-shifted absorption edges from bulk g-C_3N_4 to nanosheets and precipitates, suggesting gradually decreased π-conjugated structure. According to the above analysis, a possible exfoliation mechanism of g-C_3N_4 is proposed in Fig. 3. First, the bulk g-C_3N_4 could be partial intercalated and protonated when it was mixed with concentrated H_2SO_4. When adding water into this mixture, the rapid exothermic effect led to partial delamination and grain disintegration of g-C_3N_4 by the dissociation of weak hydrogen-bonds bridging, which in turn accelerated the intercalation of H_2SO_4 into the interlayer space of g-C_3N_4, and subsequently the -NH- linking group was cleaved and underwent oxidation under the continuous heating from further adding water, and then g-C_3N_4 was further exfoliated into smaller-sized fragments. Thus, by controlling the amount of water added, the concentration of H_2SO_4 (oxidizing strength) and heating effect can be manipulated, and hence excessive exfoliation could be avoided and g-C_3N_4 nanosheets were obtained.

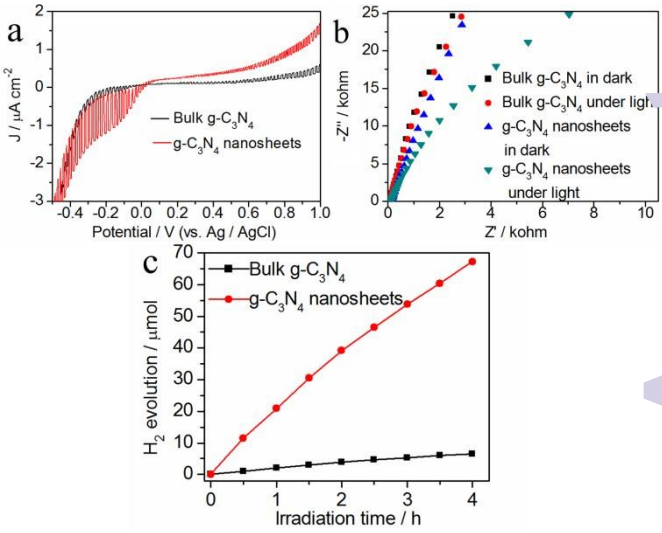

Fig. 4 (a) Photocurrent response of bulk g-C_3N_4 and g-C_3N_4 nanosheets under chopped visible light illumination (chopping frequency: 0.25 Hz, scan rate: 5 mV/s). (b) EIS plots of bulk g-C_3N_4 and g-C_3N_4 nanosheets in dark and under visible light. (c) Photocatalytic H_2 evolution over bulk g-C_3N_4 and g-C_3N_4 nanosheets under visible-light irradition (reaction conditions: 20 mg catalyst loaded with 3 wt% of Pt co-catalyst; 100 mL of H_2O containing 10 vol% triethanolamine; 210 W Xe lamp with a 400 nm cut-off filter).

In order to understand the photogenerated charge separation and transfer in as-prepared g-C_3N_4 nanosheets, which is a crucial factor for photocatalytic process, photocurrent and electrochemical impedance spectroscopy (EIS) were performed under visible light. As shown in Fig. 4a, the photocurrent generation of g-C_3N_4 nanosheets is remarkably higher than that of bulk g-C_3N_4, especially when a negative bias potential was applied, reflecting the efficient separation and transport of photoinduced electrons and holes in the g-C_3N_4 nanosheets.[13] Moreover, the negative photocurrent indicated that holes dominated the charge transport.[34] Fig. 4b shows the EIS Nyquist plots of the g-C_3N_4 nanosheets and bulk g-C_3N_4 electrodes in the dark or under visible-light irradiation. Generally, the radius of the arc on the EIS plots reflects the reaction

rate occurs on the surface of the electrode. It is found that the arc radius of g-C_3N_4 nanosheets electrode is much smaller than that of bulk g-C_3N_4 electrode both in dark and under visible light, indicating that more effective separation of photogenerated electron-hole pairs and faster interfacial charge transfer had occurred in the g-C_3N_4 nanosheets.[17] Thus, with the realization of ultrathin nanosheet structure which could reduce the bulk recombination probability of charge carriers, the as-prepared g-C_3N_4 nanosheets gained higher separation efficiency of electron-hole pairs, presenting potential application in the photocatalytic field.

The superiority of as-obtained g-C_3N_4 nanosheets for photocatalysis application was demonstrated by the photocatalytic H_2 evolution from water under visible-light irradiation ($\lambda > 400$ nm). As presented in Fig. 4c, the average hydrogen evolution rate of the g-C_3N_4 nanosheets was 840 μmol g^{-1} h^{-1}, which was more than 10 times higher than that of bulk g-C_3N_4 (82 μmol g^{-1} h^{-1}). Moreover, under the similar testing conditions, the photocatalytic activity of as-prepared g-C_3N_4 nanosheets not only outperforms the large-aspect-ratio g-C_3N_4 nanosheets fabricated in our previous work,[18] but also is superior to the single-layer g-C_3N_4 nanosheets prepared by strong acid treatment[17] and the g-C_3N_4 nanosheets synthesized by thermal oxidation exfoliation[15]. The greatly enhanced photocatalytic activity of the g-C_3N_4 nanosheets could be explained as the synergistic effects of large specific surface area, good dispersability, increased bandgap,[15] obvious defects effect[24] and improved photogenerated charge separation and transfer.

In summary, a rapid and efficient chemical exfoliation method by adding water into concentrated H_2SO_4 suspension of bulk g-C_3N_4 has been developed for the high-yield production of g-C_3N_4 nanosheets. This modified acid exfoliation method has the merits of low energy, low cost and facile control of exfoliation degree, and thus would be important in the large-scale production and extensive application of nano-sized g-C_3N_4. Compared with bulk g-C_3N_4, the as-prepared g-C_3N_4 nanosheets show great superiority in photogenerated charge separation and transfer, and consequently exhibit significantly enhanced photocatalytic activity in photocatalytic H_2 evolution from water under visible-light irradiation.

This work was financially supported by the National Natural Science Foundation of China (No. 21374106).

Notes and references

1. F. Goettmann, A. Fischer, M. Antonietti and A. Thomas, *Angew Chem Int Edit*, 2006, **45**, 4467-4471.
2. F. Goettmann, A. Fischer, M. Antonietti and A. Thomas, *New J Chem*, 2007, **31**, 1455-1460.
3. J. J. Zhu, Y. C. Wei, W. K. Chen, Z. Zhao and A. Thomas, *Chem Commun*, 2010, **46**, 6965-6967.
4. Y. Q. Sun, C. Li, Y. X. Xu, H. Bai, Z. Y. Yao and G. Q. Shi, *Chem Commun*, 2010, **46**, 4740-4742.
5. J. Liang, Y. Zheng, J. Chen, J. Liu, D. Hulicova-Jurcakova, M. Jaroniec and S. Z. Qiao, *Angew Chem Int Edit*, 2012, **51**, 3892-3896.
6. X. C. Wang, K. Maeda, A. Thomas, K. Takanabe, G. Xin, J. M. Carlsson, K. Domen and M. Antonietti, *Nat Mater*, 2009, **8**, 76-80.
7. D. J. Martin, K. P. Qiu, S. A. Shevlin, A. D. Handoko, X. W. Chen, Z. X. Guo and J. W. Tang, *Angew Chem Int Edit*, 2014, **53**, 9240-9245.
8. S. C. Yan, Z. S. Li and Z. G. Zou, *Langmuir*, 2009, **25**, 10397-10401.
9. K. Schwinghammer, M. B. Mesch, V. Duppel, C. Ziegler, J. Senker and B. V. Lotsch, *J Am Chem Soc*, 2014, **136**, 1730-1733.
10. M. Zelisko, Y. Hanlumyuang, S. B. Yang, Y. M. Liu, C. H. Lei, J. Y. Li, P. M. Ajayan and P. Sharma, *Nat Commun*, 2014, **5**.
11. X. D. Zhang, X. Xie, H. Wang, J. J. Zhang, B. C. Pan and Y. Xie, *J Am Chem Soc*, 2013, **135**, 18-21.
12. T. Y. Ma, Y. H. Tang, S. Dai and S. Z. Qiao, *Small*, 2014, **10**, 2382-2389.
13. X. J. She, H. Xu, Y. G. Xu, J. Yan, J. X. Xia, L. Xu, Y. H. Song, Y. Jiang, Q. Zhang and H. M. Li, *J Mater Chem A*, 2014, **2**, 2563-2570.
14. F. Zhao, H. H. Cheng, Y. Hu, L. Song, Z. P. Zhang, L. Jiang and L. T. Qu, *Sci Rep-Uk*, 2014, **4**.
15. P. Niu, L. L. Zhang, G. Liu and H. M. Cheng, *Adv Funct Mater*, 2012, **22**, 4763-4770.
16. S. B. Yang, Y. J. Gong, J. S. Zhang, L. Zhan, L. L. Ma, Z. Y. Fang, R. Vajtai, X. C. Wang and P. M. Ajayan, *Adv Mater*, 2013, **25**, 2452-2456.
17. J. Xu, L. W. Zhang, R. Shi and Y. F. Zhu, *J Mater Chem A*, 2013, **1**, 14766-14772.
18. J. C. Tong, L. Zhang, F. Li, M. M. Li and S. K. Cao, *Phys Chem Chem Phys*, 2015, **17**, 23532-23537.
19. X. R. Du, G. J. Zou, Z. H. Wang and X. L. Wang, *Nanoscale*, 2015, **7**, 8701-8706.
20. J. S. Zhang, M. W. Zhang, L. H. Lin and X. C. Wang, *Angew Chem Int Edit*, 2015, **54**, 6297-6301.
21. Z. Zhou, J. Wang, J. Yu, Y. Shen, Y. Li, A. Liu, S. Liu and Y. Zhang, *J Am Chem Soc*, 2015, **137**, 2179-2182.
22. L. J. Cote, F. Kim and J. X. Huang, *J Am Chem Soc*, 2009, **131**, 1043-1049.
23. Q. Su, S. P. Pang, V. Alijani, C. Li, X. L. Feng and K. Mullen, *Adv Mater*, 2009, **21**, 3191-3195.
24. V. W. H. Lau, M. B. Mesch, V. Duppel, V. Blum, J. Senker and B. V. Lotsch, *J Am Chem Soc*, 2015, **137**, 1064-1072.
25. A. Thomas, A. Fischer, F. Goettmann, M. Antonietti, J. O. Muller, R. Schlogl and J. M. Carlsson, *J Mater Chem*, 2008, **18**, 4893-4908.
26. Y. H. Zhang, Q. W. Pan, G. Q. Chai, M. R. Liang, G. P. Dong, Q. Y. Zhang and J. R. Qiu, *Sci Rep-Uk*, 2013, **3**, 1943.
27. X. D. Zhang, H. X. Wang, H. Wang, Q. Zhang, J. F. Xie, Y. P. Tian, J. Wang and Y. Xie, *Adv Mater*, 2014, **26**, 4438-4443.
28. B. B. Wang, Q. J. Cheng, L. H. Wang, K. Zheng and K. Ostrikov, *Carbon*, 2012, **50**, 3561-3571.
29. Y. C. Zhao, D. L. Yu, H. W. Zhou, Y. J. Tian and O. Yanagisawa, *J Mater Sci*, 2005, **40**, 2645-2647.
30. B. V. Lotsch and W. Schnick, *Z Anorg Allg Chem*, 2006, **632**, 1457-1464.
31. W. J. Wang, J. C. Yu, Z. R. Shen, D. K. L. Chan and T. Gu, *Chem Commun*, 2014, **50**, 10148-10150.
32. Y. J. Zhang, A. Thomas, M. Antonietti and X. C. Wang, *J Am Chem Soc*, 2009, **131**, 50-51.
33. X. J. Bai, S. C. Yan, J. J. Wang, L. Wang, W. J. Jiang, S. L. Wu, C. P. Sun and Y. F. Zhu, *J Mater Chem A*, 2014, **2**, 17521-17529.
34. Y. J. Zhang, T. Mori, J. H. Ye and M. Antonietti, *J Am Chem Soc*, 2010, **132**, 6294-6295.